CHIN. PHYS. LETT. Vol. 37, No. 1 (2020) 014501 **Express Letter**

Coherent Transfer of Excitation in a Nanomechanical Artificial Lattice *

Liang Zhang(张亮)[1,2], Tian Tian(田添)[1,2], Pu Huang(黄璞)[3],
Shaochun Lin(林劭春)[1,2], Jiangfeng Du(杜江峰)[1,2,4**]

[1]*CAS Key Laboratory of Microscale Magnetic Resonance and Department of Modern Physics, University of Science and Technology of China, Hefei 230026*
[2]*Synergetic Innovation Center of Quantum Information and Quantum Physics, University of Science and Technology of China, Hefei 230026*
[3]*National Laboratory of Solid State Microstructures and Department of Physics, Nanjing University, Nanjing 210093*
[4]*Hefei National Laboratory for Physical Sciences at the Microscale, University of Science and Technology of China, Hefei 230026*

(Received 31 October 2019)

We realize a coherent transfer of mechanical excitation in a finely controlled artificial nanomechanical lattice. We also realize strong dynamic coupling between adjacent high-Q mechanical resonators, via modulated dielectric force at the frequency difference between them. An excitation transfer across a lattice consisting of 7 nanobeams is observed by applying a design sequence of switching for couplings, with the final effective population reaching 0.94. This work not only demonstrates the ability to fully control an artificial lattice but also provides an efficient platform for studying complicated dynamics in one-dimensional systems.

PACS: 45.80.+r, 34.50.Ez, 05.45.Xt DOI: 10.1088/0256-307X/37/1/014501

Nanomechanical systems have unique potential to achieve so-called artificial lattices, compared to optical microtraps,[1,2] cavities,[3] Rydberg atoms,[4,5] and some other systems. Recently, remarkable advances have been made in strong couplings of several mechanical modes, where the coherent excitation transfer between the modes is demonstrated.[6–10] However, these manufactured structures face considerable difficulties in terms of scalability, thus the coherent excitation transfer across multiple modes remains unimplemented. Nowadays, the development of nanotechnology enables us to arrange the nanobeams close enough, which makes it possible to realize strong and tunable dielectric couplings between adjacent mechanical resonators.[11] As a start, the coherent excitation transfer across the coupled modes plays an essential role in rehearsing a practical artificial lattice. Moreover, the implemented system provides powerful tools for forming quantum and classical models in the fields of topological phase transition,[12–15] many-body systems,[16,17] programmable logic devices,[18] and so on.

In this Letter, we report a coherent excitation transfer across an artificial nanomechanical lattice, where the nearest-neighbor couplings are fully controlled. The fundamental flexural modes of adjacent nanobeams are coupled via the dielectric forces generated from the applied static and dynamic voltages. The strong coupling enables the much faster coherent energy exchange than the mechanical dissipation. Under this strong coupling condition, the physical mechanism of coupled multi-modes is analogous to an N-level quantum system. More importantly, the nearest-neighbor couplings are linearly controllable. We could finely control the couplings between arbitrary adjacent modes to implement an actual artificial lattice with versatile applications. We design a sequence for individual switching the couplings in the lattice to route the excitation transfer. The scalability of the proposed scheme is also discussed.

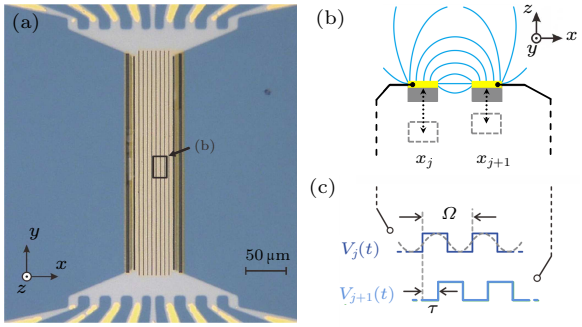

Fig. 1. Artificial nanomechanical lattice. (a) Microscope graph of the suspending Si_3N_4 nanobeams (dark yellow), the size of each is 200 μm × 3 μm × 100 nm. For applying the voltages, 10-nm-thick Au is coated on the nanobeams. The external electrodes (yellow) are 100-nm-thick Au. The thickness of the Si_3N_4 substrate (dark blue) is 300 μm. (b) The cross sections of adjacent resonators, indicating the two nanobeams inside the black box in (a). When applied dc and ac voltages on the Au layer, the oscillation of the resonator could coherently transfer to another via dynamic coupling method. The blue lines represent the generated electric field. (c) Examples of controlling coupling strengths dynamically, switching (solid line) and modulating (dashed line).

The nanomechanical artificial lattice shown in Fig. 1(a) consists of 7 side-by-side double-clamped high-stress Si_3N_4 nanobeams. The natural eigenfrequencies of the fundamental out-of-plane modes have

*Supported by the National Key R&D Program of China under Grant No. 2018YFA0306600, the Key Research Program of Frontier Sciences of CAS under Grant No. QYZDY-SSW-SLH004, the Key R&D Team of CAS under Grant No. GJJSTD20170001, and Anhui Initiative in Quantum Information Technologies under Grant No. AHY050000.
**Corresponding author. Email: djf@ustc.edu.cn

slight deviations around 1 MHz, $\omega_0 \sim 2\pi \times 1$ MHz. Benefit from the vacuum ambiance at 10^{-7} mBar and at low temperature 4 K, the decay rates of these flexural modes are as small as $\gamma < 2\pi \times 10$ Hz, which means that the quality factors Q exceed 1×10^5. The sample is fabricated using typical silicon/Si_3N_4 based processing technologies (for details see Note 1 in the Supplementary Material). The motions of adjacent resonators are coupled via modulated dielectric force,[11] as shown by the schematic diagram in Fig. 1(b). By applying a dc voltage $V^{\rm dc}$, the static coupling between adjacent nanobeams is realized. However, this coupling cannot transfer the excitation coherently between the resonators because of their eigenfrequency difference and narrow bandwidth. To overcome this problem, we employ the so-called dynamic coupling method,[15,18,19,20] an ac pump voltage $V_n^{\rm p}$ is combined with $V^{\rm dc}$ via a low-frequency bias-tee, at the frequency difference of the neighbor resonators, $\omega_n^{\rm p} = \omega_{n+1} - \omega_n$. The interacting dielectric force on the nth nanobeam is expressed as

$$\begin{aligned} F_n^{\rm elec} &= m_n K_n(t)(x_{n+1} - x_n) \\ &= gV^{\rm dc}V_n^{\rm p}\cos(\omega_n^{\rm p}t)(x_{n+1} - x_n), \end{aligned} \tag{1}$$

where $K_n(t)$ is dynamic coupling strength and g is a geometric factor related to the shape, size and induced electric field of the fabricated nanobeams. Typically, the frequency difference is far less than the eigenfrequency, $\omega_n^{\rm p} \ll \omega_0$. As we reported earlier,[15] K_n is proportional to the applied $V_n^{\rm ac}(t)$ when $V^{\rm dc}$ is fixed. This significant linearly relationship brings broader dynamical controllability to the independent coupling strength, such as switching, modulating, and ramping, as shown in Fig. 1(c).

Experimental characterization of the lattice is shown in Figs. 2(a) and 2(b). We measure the response spectra of coupled and uncoupled nanomechanical resonators by using the magnetomotive technique (also see the Supplementary Material).[21–23] The device is located in a uniform magnetic field along the x direction (Fig. 1(a)) $B = 1$ T. Thus the driving Lorentz force $F_{\rm D} = I_{\rm D}LB$ is generated when a current passes through the nanobeam. Meanwhile, the excited motion, perpendicular to the field, produces an electromotive force across the nanobeam. Steady-state response of $V_{\rm EMF}(\omega)$ vs $I_{\rm D}(\omega)$ is demodulated by a high frequency lock-in amplifier (Zurich Instruments, HF2LI), fitted by the formula

$$V_{\rm EMF}(\omega) = \frac{i\xi\omega L^2B^2/m}{\omega_0^2 - \omega^2 + i\omega\omega_0/Q} I_{\rm D}(\omega), \tag{2}$$

where ξ is a shape factor depending on the mode, being about 0.81 for the fundamental mode of a high-tension resonator (also see the Supplementary Material).[22] In the absence of $V^{\rm dc}$ and $V_n^{\rm p}$, the dissipative rate (i.e., the decay rate) of an uncoupled resonator is obtained by the full width at half maximum (FWHM) of response spectrum, as shown in Fig. 2(a) (top panel), with a typical value $\gamma < 10$ Hz.

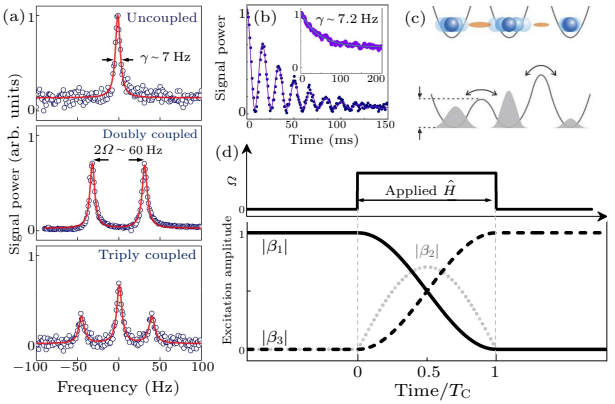

Fig. 2. Characterization of the device and transfer scheme. (a) The response spectra (circles) are read out using a lock-in amplifier, fitted with Lorentzian function (solid red lines). The applied large dc voltage $V^{\rm dc}$ is fixed to 8 V. Top: the spectrum of single uncoupled mode, the fitted FWHM is about 7.0 Hz. Middle: dynamic coupled two modes with $V^{\rm p} = 200$ mV, the splitting of peaks indicates the effective coupling strength of 30 Hz. Bottom: dynamic coupled three modes (cascaded, 1–2–3), measured on the first one of the three resonators. (b) The coherent Rabi oscillations between doubly coupled modes in (a). The inset is the time-domain decay signal of an uncoupled mode, the decay rate is about 7.2 Hz by fitting this curve. (c) The strong dynamic coupling resonators are analogous to a single particle in a multi-well potential. (d) The scheme of transfer process in the three coupled resonators. The time unit $T_{\rm C}$ is $\sqrt{2}\pi/\Omega$. Upper: the control sequence, where we apply the effective 'gate' $\hat{H}$ from $t = 0$ to $t = T_{\rm C}$. Lower: the time-domain excitation amplitudes on different resonators, i.e., $|\beta_n|$.

To realize the dynamic coupling between the resonators, we fix $V^{\rm dc}$ as large as 8 V and apply a sufficient pumping voltage $V^{\rm p} \sim 200$ mV on one of the nanobeams. When the pumping signal is at the frequency difference $\omega^{\rm p} = \omega_2 - \omega_1$, we can observe a normal mode splitting in the spectrum, indicating the effective coupling strength $\Omega_n = K_n/2 = 2\pi \times 30$ Hz, as shown in Fig. 2(a) (middle panel). For three adjacent resonators, we apply the static and dynamic voltages on the middle nanobeam. The $V^{\rm dc}$ remains fixed to 8 V, with $V_1^{\rm ac}$ and $V_2^{\rm ac}$ combined simultaneously. In general, the $V_n^{\rm ac}$ requires finely tuned to ensure that the effective coupling strength Ω_n is uniform ($2\pi \times 30$ Hz). The spectrum of three normal modes is observed when the pumping frequencies equal to respective frequency differences, as shown in Fig. 2(a) (bottom panel). Furthermore, we test the coherent Rabi oscillations[6] and the damped exponential signal to verify the coupling strength and decay rate, as shown in Fig. 2(b).

The dynamic coupling method enables the coherent transfer of mechanical excitation between adjacent resonators. However, the process in a lattice is more complicated. We consider the motion of three dynamic-coupled nanomechanical resonators, assuming that they are nearly identical,

$$\begin{aligned} &\ddot{x}_1 + \gamma_1\dot{x}_1 + \omega_1^2 x_1 = K_1(t)(x_2 - x_1), \\ &\ddot{x}_2 + \gamma_2\dot{x}_2 + \omega_2^2 x_2 = K_1(t)(x_1 - x_2) + K_2(t)(x_3 - x_2), \end{aligned}$$

$$\ddot{x}_3 + \gamma_3 \dot{x}_3 + \omega_3^3 x_3 = K_2(t)(x_2 - x_3), \tag{3}$$

where ω_n is the eigenfrequency, $K_n(t) = K_n \cos(\omega_n^{\rm p} t)$ is the dynamic coupling strength with $\omega_n^{\rm p}$ being the pump frequency, $\gamma_n = \omega_n/Q_n$ is the decay rate with Q_n being the quality factor. In this study, K_n is much larger than γ_n, which agrees with the strong-coupling condition. When the pump signal is applied at $\omega_n^{\rm p} = \omega_{n+1} - \omega_n$, we could introduce the rotating-wave approximation into Eq. (3). Then the reduced equations of demodulated complex amplitudes $\{\psi_n(t)\}$ is similar to the quantum Schrödinger equation describing a single particle in a multi-well potential like Fig. 2(c),[6,24,25] namely,

$$i \begin{pmatrix} \dot{\psi}_1 \\ \dot{\psi}_2 \\ \dot{\psi}_3 \end{pmatrix} = \begin{pmatrix} -i\frac{\gamma_1}{2} & \Omega_1 & 0 \\ \Omega_1 & -i\frac{\gamma_2}{2} & \Omega_2 \\ 0 & \Omega_2 & -i\frac{\gamma_3}{2} \end{pmatrix} \begin{pmatrix} \psi_1 \\ \psi_2 \\ \psi_3 \end{pmatrix}, \tag{4}$$

where $x_n = \Re[\psi_n e^{i\omega_n t}]$. We adjust the effective coupling strength $\Omega_n = K_n/4\omega_n$ to be consistent, reaching $\Omega = 2\pi \times 30\,\text{Hz}$. This mapping is still valid in the case of multi-coupled resonators.[15,26,27]

We adopt the quantum mechanics methods to make a clear description of the dynamics of Eq. (4). Under the approximation that the decay rates of all resonators are nearly equal, $\gamma_n \approx \gamma$, the diagonal damping terms can be neglected by assuming a normalized 'wavefunction', $|\phi(t)\rangle = \frac{1}{A(t)}|\psi(t)\rangle = \frac{1}{A(t)}(\psi_1, \psi_2, \psi_3)^{\rm T}$. Here $A(t) = \sqrt{\sum |\psi_n^2|} \sim A(0)\exp(-\gamma t/2)$ is the normalization factor, mainly involving the dissipation. Actually, the standard deviation of the experimental measured decay rates is about 0.5 Hz, satisfying the approximation (for detailed experimental and numerical results see Note 2 in the Supplementary Material). Now Eq. (4) is rewritten in the form of quantum mechanics without dissipation,

$$i|\dot{\phi}\rangle = \hat{H}|\phi\rangle, \quad \hat{H} = \begin{pmatrix} 0 & \Omega & 0 \\ \Omega & 0 & \Omega \\ 0 & \Omega & 0 \end{pmatrix}, \tag{5}$$

where $\hat{H}$ is the effective Hamiltonian. Obviously, the solution to Eq. (5) is $|\phi(t)\rangle = \sum \alpha_n |\phi_n\rangle \exp(-i\epsilon_n t)$, where $\alpha_n = \langle\phi_n|\phi(0)\rangle$ with $|\phi_n\rangle$, ϵ_n being the eigenvectors and eigenvalues of $\hat{H}$, respectively. We use a set of natural bases $\{|n\rangle\}$ to represent $|\phi(t)\rangle$, $|\phi(t)\rangle = \sum \beta_n(t)|n\rangle$ with $|n\rangle$ denoting $(0, \ldots, 0, 1, 0, \ldots, 0)^{\rm T}$. The coefficient β_n represents the normalized complex amplitude of the nth resonator, equivalent to the probability amplitudes, $\sum |\beta_n|^2 = 1$. Figure 2(d) shows the excitation amplitudes $\{|\beta_n|\}$ versus time, demonstrating the coherent transfer of excitation from the 1st nanobeam to the 3rd nanobeam at a certain time $T_{\rm C} = \sqrt{2}\pi/\Omega$. We represent this transfer as $|\phi(0)\rangle = (1, 0, 0)^{\rm T} \to |\phi(T_{\rm C})\rangle = (0, 0, -1)^{\rm T}$, with a π phase flip theoretically. The demodulated phase in β_n represents the accumulated phase of the system in the process. However, these phases play little significance because the eigenfrequencies of these resonators are inconsistent in experiment. This is also because we cannot ensure that all pump signals have the same initial phase.

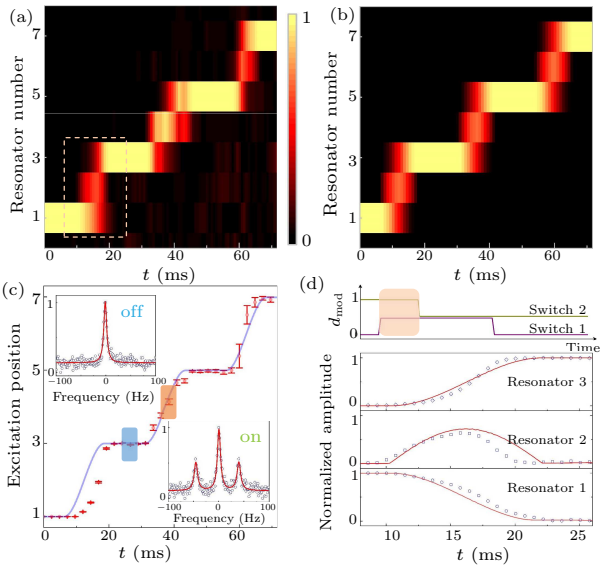

Fig. 3. Coherent excitation transfer in the lattice. (a) The measured normalized excitation amplitudes of each resonator versus time in the experiment. The typical transfer across a unit cell is shown in (d), refer to the dashed box. The amplitudes are normalized. (b) Numerical results for (a) without dissipation. The color bar of (a) and (b) is between them. (c) The equivalent location of a single excitation transferred (red points), and the error bars indicate one standard deviation. The solid blue line is the design trajectory. The insets show the spectra of nanobeam 3 when the switch of coupling is turned on or off. The vertical axis represents the signal power (arb. units), while the horizontal axis represents the frequency in units of Hz. (d) The dynamics of the 1st unit cell, pointing to the dashed box in (a). Upper: the stagger sequence of two switches for coupling, the front switch is applied later to avoid diversion. Lower: the normalized amplitude $|\beta_n|$ (dots), with the error bars smaller than the data points. The solid lines are predicted trajectories under the design control sequences.

The above scheme of excitation transfer has a good scalability because of the dynamic coupling technique, which only requires the fabricated nanobeams to be approximately identical. Thus, we experimentally extend the unit cell composed of three nanomechanical resonators into an artificial lattice with 3 unit cells end to end (7 nanobeams totally). To implement an efficient transfer in this lattice, we need individual switching for the applied effective $\hat{H}$ on each unit cell. Equation (1) reveals that we could control the nearest-neighbor coupling K_n by turning-on and off the pump voltage $V_n^{\rm P}$. Furthermore, we design a stagger sequence for controlling the adjacent couplings to avoid the diversion in lattice. We apply the front pump voltage $V_{n-1}^{\rm P}$ after $V_n^{\rm P}$ for the nth resonator, as shown in Fig. 3(d). In experiment, this control sequence avoids the effect of the imprecise control

gate in a long lattice, resulting in a coherent transfer from $|\phi(0)\rangle = (1, 0, \ldots)^{\mathrm{T}}$ to $|\phi(t)\rangle = (0, \ldots, 0.97)^{\mathrm{T}}$, as shown in Fig. 3(a), which agrees well with the numerical results in Fig. 3(b). Thus the final effective population is $|\beta_7|^2 \approx 0.94$.

We directly demodulate the vibration signal of nanomechanical resonators to obtain the time-dependent amplitude $r_n(t)$ with its phase $\varphi_n(t)$ using the lock-in amplifier, thus $\psi_n(t) = r_n e^{i\varphi_n}$. For the mentioned normalized complex amplitude β_n, we have the following normalization at each point in measurement,

$$\beta_n(t) = \frac{\psi_n(t)}{\sqrt{\sum |\psi_n|^2}}. \tag{6}$$

In this work, the total time measured is 72 ms with the decoherence time of the system being about 150 ms, and the measured amplitude of final signal on nanobeam 7 is still much larger than the baseline noise. Thus the normalization (6) is valid for the entire measurement.

When the excitation signal transmits in the lattice, we calculate the equivalent location to represent the transfer of mechanical energy, defined by

$$P(t) = \sum_n |\beta_n(t)|^2 n, \tag{7}$$

as shown in Fig. 3(c). We observe that the designed control sequence guarantees the accuracy of the applied effective gates well, even with intrinsic fluctuations in the fabricated device and pump voltages. Meanwhile, the detailed dynamics in each unit cell is in good agreement with the predicted lines, as shown in Fig. 3(d).

Now we perform a simple extension to a much larger nanomechanical lattice with 31 resonators (16 unit cells end to end) in a numerical simulation. Employing the same coupling scheme and controlling sequence, we coherently transfer the excitation between the frontiers of the lattice, as shown in Fig. 4(a). However, we find that in a sufficient extended lattice, the dissipation will destroy the transfer. The final signal on resonator 31 is as small as −70 dB of the initial excitation, as shown in Fig. 4(b) (light yellow bars and blue line and dots). The signal decay is extremely hard to avoid, due to the finite quality factor of nanomechanical resonators. Meanwhile, the initial excitation strength is also limited by the nonlinear effects of nanobeams. Alternatively, we could build some nanomechanical relay amplifiers in the lattice.

The nanomechanical parametric amplification between two adjacent resonators is realized by applying the pump voltage $V_n^{\mathrm{p}}(t)$ at a high frequency.[28,29] When $K_n(t) = K_n \cos(\omega_n^{\mathrm{p}} t)$ is applied at $\omega_n^{\mathrm{p}} = \omega_n + \omega_{n+1}$, the vibration of the adjacent resonator is dynamic amplified with phase preserving, i.e., the so-called non-degenerate parametric amplification.[30−33] Here we employ the parametric amplifier as relay amplifiers in the artificial lattice, locating at the end of every two unit cells. By setting an appropriate pump voltage, we make the amplifier gain regular in finite time $G = 11.6$ dB to cover the dissipation without varying the control sequence. The numerical results are shown as gray bars in Fig. 4(b), with the same results in units of dB shown by red dots. Using relay amplifier shows much more feasible than enhancing the quality factor of nanobeams, or actuating strong initial excitation. The amplifier requires much smaller pump voltage than the couplings, since the gain is sensitive to the pump voltages. However, when the pump voltage approaches the critical point, this amplifier will enter the unstable range, where the sensitivity is greatly enhanced (for detailed simulation see Note 3 in the Supplementary Material). The place and gain of these relay amplifiers should be appropriately set in experiments.

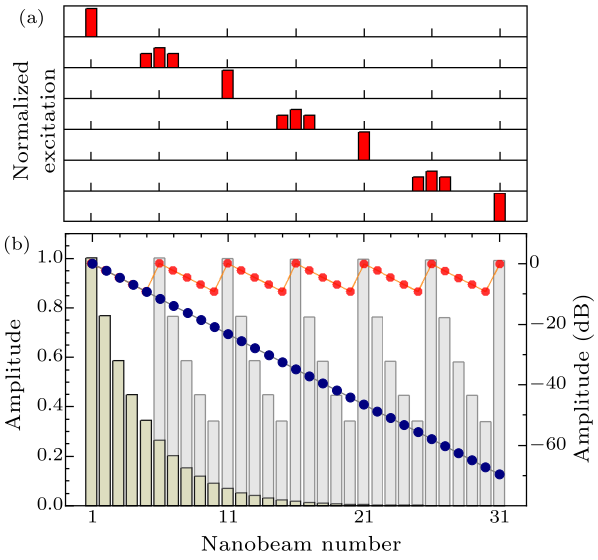

Fig. 4. Numerical extension to a larger lattice with 16 unit cells, $N = 31$. (a) The normalized excitation amplitude during the transfer. The vertical axis of each frame ranges from 0 to 1.1 unit amplitude. The total transfer time is about 360 ms, under the same coupling strength in our experiment. (b) Light yellow bars: the intrinsic amplitudes on each resonator, with the same decay rate 7.2 Hz in our experiment. The final excitation signal is about −70 dB of the initial. Blue dots show the decaying amplitudes in units of dB. Gray bars: the amplitudes of resonators using relay amplification. The signal is amplified at the end of every two unit cells. The red dots show the amplitudes in units of dB.

Combined with the controllable couplings and direct observation of vibrating amplitudes, the implemented lattice takes advantage of studying one-dimensional (1D) topological systems under open boundary conditions. For example, considering Eqs. (4) and (5), the staggered couplings Ω_n make the lattice conform the Su-Schrieffer–Heeger (SSH) model, the simplest 1D lattice with topology.[34] Furthermore, the dynamics of wavefunction could be reconstructed by observing the time-dependent amplitudes of each resonator. This lattice can also be used to study some non-Hermitian systems. If we manually control the

decay rates staggered around the same value $\gamma+\gamma_1$, $\gamma-\gamma_2$, the effective Hamiltonian (5) with incorporating gain and loss is established, which is often used to study the PT-symmetry.[35]

In summary, we have implemented a strong-coupling artificial lattice consisting of multiple high-Q nanomechanical resonators using dynamic dielectric force between adjacent nanobeams. We propose a scalable scheme for excitation transfer in the artificial lattice and experimentally demonstrate it with $N=7$. We perform the experiments at temperature 4K and the device is integrated into a small chip with the size 3mm × 3mm, which needs to be emphasized that the functional area size is 100 μm square. To practically extend this scheme, we provide a solution to avoid the influence of dissipation on excitation transfer in a large lattice and verify it by numerical results.

In addition, we finely control the couplings in the lattice and make a direct observation on vibrations of nanobeams, which enables many applications on 1D topological or N-level systems, despite classical domain. For example, some topological effects in mechanical systems are reported and predicted,[36–38] the simulation on population transfer in multi-level systems is also available.[39–41] Furthermore, the implemented system has potential for observing complicated dynamics in the fields of phase transition,[42] artificial gauge fields[43,44] and exotic states.[45]

We thank Yongguan Ke, Chaohong Lee, Jiangbin Gong, Changkui Duan for helpful discussion.

References

[1] Bloch I 2005 *Nat. Phys.* **1** 23
[2] Eckardt A 2017 *Rev. Mod. Phys.* **89** 011004
[3] Umucalılar R O and Carusotto I 2011 *Phys. Rev. A* **84** 043804
[4] de Léséleuc S, Lienhard V, Scholl P, Barredo D, Weber S, Lang N, Büchler H P, Lahaye T and Browaeys A 2019 *Science* **365** 775
[5] Omran A, Levine H, Keesling A, Semeghini G, Wang T T, Ebadi S, Bernien H, Zibrov A S, Pichler H, Choi S, Cui J, Rossignolo M, Rembold P, Montangero S, Calarco T, Endres M, Greiner M, Vuletić V and Lukin M D 2019 *Science* **365** 570
[6] Faust T, Rieger J, Seitner M J, Kotthaus J P and Weig E M 2013 *Nat. Phys.* **9** 485
[7] Deng G W, Zhu D, Wang X H, Zou C L, Wang J T, Li H O, Cao G, Liu D, Li Y, Xiao M, Guo G C, Jiang K L, Dai X C and Guo G P 2016 *Nano Lett.* **16** 5456
[8] Mathew J P, Patel R N, Borah A, Vijay R and Deshmukh M M 2016 *Nat. Nanotechnol.* **11** 747
[9] Zhu D, Wang X H, Kong W C, Deng G W, Wang J T, Li H O, Cao G, Xiao M, Jiang K L, Dai X C, Guo G C, Nori F and Guo G P 2017 *Nano Lett.* **17** 915
[10] Gajo K, Schüz S and Weig E M 2017 *Appl. Phys. Lett.* **111** 133109
[11] Unterreithmeier Q P, Weig E M and Kotthaus J P 2009 *Nature* **458** 1001
[12] Aidelsburger M, Lohse M, Schweizer C, Atala M, Barreiro J T, Nascimbène S, Cooper N R, Bloch I and Goldman N 2015 *Nat. Phys.* **11** 162
[13] Drost R, Ojanen T, Harju A and Liljeroth P 2017 *Nat. Phys.* **13** 668
[14] Leykam D, Andreanov A and Flach S 2018 *Adv. Phys.: X* **3** 1473052
[15] Tian T, Ke Y, Zhang L, Lin S, Shi Z, Huang P, Lee C and Du J 2019 *Phys. Rev. B* **100** 024310
[16] Guardado-Sanchez E, Brown P T, Mitra D, Devakul T, Huse D A, Schauß P and Bakr W S 2018 *Phys. Rev. X* **8** 021069
[17] Harris R, Sato Y, Berkley A J, Reis M, Altomare F, Amin M H, Boothby K, Bunyk P, Deng C, Enderud C, Huang S, Hoskinson E, Johnson M W, Ladizinsky E, Ladizinsky N, Lanting T, Li R, Medina T, Molavi R, Neufeld R, Oh T, Pavlov I, Perminov I, Poulin-Lamarre G, Rich C, Smirnov A, Swenson L, Tsai N, Volkmann M, Whittaker J and Yao J 2018 *Science* **361** 162
[18] Huang P, Zhang L, Zhou J, Tian T, Yin P, Duan C and Du J 2016 *Phys. Rev. Lett.* **117** 017701
[19] Huang P, Wang P, Zhou J, Wang Z, Ju C, Wang Z, Shen Y, Duan C and Du J 2013 *Phys. Rev. Lett.* **110** 227202
[20] Okamoto H, Schilling R, Schütz H, Sudhir V, Wilson D J, Yamaguchi H and Kippenberg T J 2016 *Appl. Phys. Lett.* **108** 153105
[21] Cleland A and Roukes M 1999 *Sens. Actuators A* **72** 256
[22] Poot M and van der Zant H S 2012 *Phys. Rep.* **511** 273
[23] Imboden M and Mohanty P 2014 *Phys. Rep.* **534** 89
[24] Novotny L 2010 *Am. J. Phys.* **78** 1199
[25] Seitner M J, Ribeiro H, Kölbl J, Faust T and Weig E M 2017 *New J. Phys.* **19** 033011
[26] Briggs J S and Eisfeld A 2012 *Phys. Rev. A* **85** 052111
[27] Skinner T E 2013 *Phys. Rev. A* **88** 012110
[28] Louisell W H 1960 *Coupled Mode and Parametric Electronics* (New York: Wiley)
[29] Olkhovets A, Carr D, Parpia J and Craighead H 2001 *IEEE 14th IEEE International Conference on Micro Electro Mechanical Systems* **2001** 01CH37090
[30] Clerk A A, Devoret M H, Girvin S M, Marquardt F and Schoelkopf R J 2010 *Rev. Mod. Phys.* **82** 1155
[31] Bergeal N, Schackert F, Metcalfe M, Vijay R, Manucharyan V E, Frunzio L, Prober D E, Schoelkopf R J, Girvin S M and Devoret M H 2010 *Nature* **465** 64
[32] Abdo B, Kamal A and Devoret M 2013 *Phys. Rev. B* **87** 014508
[33] O'Brien K, Macklin C, Siddiqi I and Zhang X 2014 *Phys. Rev. Lett.* **113** 157001
[34] Asbóth J K, Oroszlány L and Pályi A 2016 *A Short Course on Topological Insulators* (Berlin: Springer International Publishing)
[35] El-Ganainy R, Makris K G, Khajavikhan M, Musslimani Z H, Rotter S and Christodoulides D N 2018 *Nat. Phys.* **14** 11
[36] Süsstrunk R and Huber S D 2015 *Science* **349** 47
[37] Chen H, Nassar H and Huang G 2018 *J. Mech. Phys. Solids* **117** 22
[38] Chien C C, Velizhanin K A, Dubi Y, Ilic B R and Zwolak M 2018 *Phys. Rev. B* **97** 125425
[39] Oreg J, Bergmann K, Shore B W and Rosenwaks S 1992 *Phys. Rev. A* **45** 4888
[40] Felicetti S, Romero G, Rossini D, Fazio R and Solano E 2014 *Phys. Rev. A* **89** 013853
[41] Kandel Y P, Qiao H, Fallahi S, Gardner G C, Manfra M J and Nichol J M 2019 *Nature* **573** 553
[42] Ludwig M and Marquardt F 2013 *Phys. Rev. Lett.* **111** 073603
[43] Dalibard J, Gerbier F, Juzeliūnas G and Öhberg P 2011 *Rev. Mod. Phys.* **83** 1523
[44] Struck J, Weinberg M, Ölschläger C, Windpassinger P, Simonet J, Sengstock K, Höppner R, Hauke P, Eckardt A, Lewenstein M and Mathey L 2013 *Nat. Phys.* **9** 738
[45] Matheny M H, Emenheiser J, Fon W, Chapman A, Salova A, Rohden M, Li J, de Badyn M H, Pósfai M, Duenas-Osorio L, Mesbahi M, Crutchfield J P, Cross M C, D'Souza R M and Roukes M L 2019 *Science* **363** eaav7932